Letter

Pure transverse spin perpendicular to wave propagation in multiple plane waves

Yuanlu Chen,[1] Yaxin Li,[2] Bijun Xu,[1,*] Xiaogang Wang,[1] Jun Chen,[2,3,†] Zhifang Lin,[4,5] and Xinning Yu[1,‡]

[1]*School of Science, Zhejiang University of Science and Technology, Hangzhou 310023, China*

[2]*State Key Laboratory of Quantum Optics and Quantum Optics Devices, Institute of Theoretical Physics, Shanxi University, Taiyuan 030006, China*

[3]*Collaborative Innovation Center of Extreme Optics, Shanxi University, Taiyuan 030006, China*

[4]*State Key Laboratory of Surface Physics (SKLSP), Key Laboratory of Micro and Nano Photonic Structures (Ministry of Education), and Department of Physics, Fudan University, Shanghai 200433, China*

[5]*Collaborative Innovation Center of Advanced Microstructures, Nanjing University, Nanjing 210093, China*

(Received 31 August 2023; revised 20 November 2023; accepted 22 November 2023; published 15 December 2023)

Transverse spin, an intriguing aspect of spin angular momentum, has gained considerable attention in recent years. However, transverse spin is typically accompanied by longitudinal spin in electromagnetic fields. This work aims to generate a series of optical fields with pure transverse spin. We present analytical and numerical demonstrations showing that when multiple linearly polarized plane waves interfere in the same plane, the longitudinal spin vanishes, leaving only the transverse spin, which is perpendicular to both the wave propagation and the inhomogeneous field plane. This transverse spin is demonstrated to be related to the imaginary part of the complex Poynting momentum. Furthermore, we show that pure transverse spin is also observed in the interference of multiple Gaussian beams, offering practical applications in optical field preparation and enhancing our understanding of spin-related physics.

DOI: 10.1103/PhysRevB.108.L241112

Introduction. Spin angular momentum (SAM), which encompasses both longitudinal and transverse components [1,2], is a fundamental dynamic property of electromagnetic fields [3–8]. The longitudinal spin (L spin), a helix-dependent component, aligns along the local wave vector (**k**). On the other hand, the transverse spin (T spin), a helix-independent component, is perpendicular to the local wave vector and is locked by the momentum, giving rise to the concept of spin-momentum locking [5,9,10]. In physics, the T spin is related to the inhomogeneity of momentum distribution in the optical field [11–14]. The unique physical characteristics and orientation of T spin, distinguished from L spin, provide new avenues for manipulation, sparking research interest in a wide range of fascinating phenomena, such as optical manipulation [15–20], laser cooling [21], unidirectional guided waves [22], imaging [23–25], and communications [26]. In addition, metasurfaces, which flexibly control the spatial structure of SAM in the light, open new paths for T-spin-based applications in ultracompact nanophotonic platforms [27–30].

However, in most optical fields, the emphasis is on the L spin, while the T spin tends to be overlooked [31–34]. This is primarily because, for instance, the intense T spin is confined to a narrow region when the optical fields are tightly focused, whereas the L spin extensively persists. [35–37]. The persistence of the L spin can be attributed to the presence of the intrinsic or interference-generated helix in these interference fields [38]. While T spins can be generated in fields such as surface-plasmon polaritons, they depend highly on the designed medium [27,28,30,39]. Furthermore, the evanescent fields with a pure T spin are experimentally practical only within the near-field range [2,22,35,40,41]. Consequently, exploring optical fields that carry a pure T spin with an extensive range is urgently needed.

In this Letter, we present a study on optical fields carrying pure T spin perpendicular to wave propagation while the L-spin component vanishes and the total SAM is locked by momentum [40,42–44]. In this case, the lateral component of Belinfante's spin momentum (BSM) disappears [40,42–44]. As a result, the T spin aligns itself along a direction where momentum symmetry is preserved, and the light does not exhibit any field gradient or propagation characters in this lateral direction. Therefore, this T spin is perpendicular to both the wave propagation and the inhomogeneous field plane. We provide an analytical derivation on the general case of plane-wave interference, which leads to the pure T spin under certain conditions. The results are applicable universally and are not restricted to specific physical parameters such as complex amplitude, propagation direction, or the number of plane waves. In the case of an interference field with pure T spin, the relationship between the T-spin density and the imaginary Poynting momentum (imaginary part of the complex Poynting momentum) density is established to study the intricate interplay between the T spin and optical forces [15,38,40,45–47]. Furthermore, the robustness of pure T spin in the quasi-optical lattice [48–50] formed by Gaussian beams [35,51,52] further support the practical implications of our study.

*xubijun@zust.edu.cn
†chenjun@sxu.edu.cn
‡xinning_yu@fudan.edu.cn

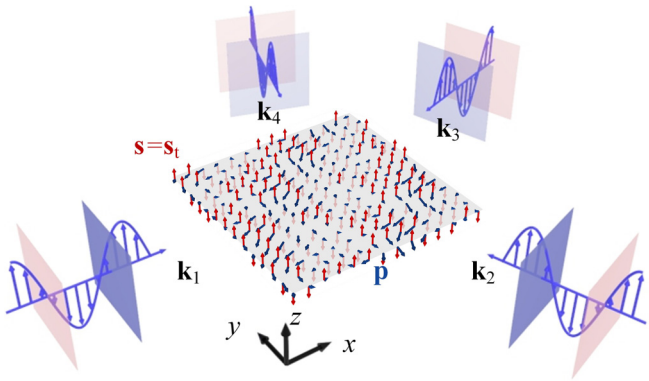

FIG. 1. The pure T spin is perpendicular to wave propagation and locked by the momentum, in an optical field composed of four plane waves with all the wave vectors lying in the xy plane and sharing the same polarization vector. The total SAM density vector and the momentum density vector on the $z = 0$ plane are represented by red and blue arrows, respectively. It is obvious that the T-spin density are all along the z direction and the momentum density lying in the xy plane. The parameters of the four plane waves are set as $m_i = 1, A_i = 1,\ \mathrm{i},\ 1+\mathrm{i},\ 1-\mathrm{i}$, and $\beta_i = 0^\circ,\ 108^\circ,\ 198^\circ,\ 252^\circ$ for $i = 1,\ 2,\ 3,\ 4$, respectively.

Results and discussion. To illustrate the pure T spin, let us consider an optical field composed of n_p plane waves. Figure 1 depicts a schematic plot of this field for a specific case where $n_p = 4$. In this scenario, the n_p plane waves all have the same wavelength, and their wave vectors are confined to the xy plane. The electric field of a general optical field composed of n_p plane waves can be expressed as [40,53,54]

$$\mathbf{E} = \sum_i^{n_p} \mathbf{E}_i = \sum_i^{n_p} U_i \boldsymbol{\mathcal{E}}_i e^{\mathrm{i}\mathbf{k}_i\cdot\mathbf{r}}, \tag{1}$$

where $U_i = A_i/(1+|m_i|^2)^{1/2}$ is the normalized amplitude of each wave. The position vector $\mathbf{r} = x\mathbf{e}_x + y\mathbf{e}_y + z\mathbf{e}_z$, where $\mathbf{e}_x$, $\mathbf{e}_y$, and $\mathbf{e}_z$ are the unit vectors in the Cartesian coordinate. The wave vector $\mathbf{k}_i = k\cos\beta_i\mathbf{e}_x + k\sin\beta_i\mathbf{e}_y$, where k represents the wave number in the background medium, given by $k = 2\pi/\lambda$, with λ being the wavelength. The variables β_i correspond to the angles that determine the direction of the wave vector $\mathbf{k}_i$ in the xy plane. In this optical field, the phase of the plane wave $\mathbf{k}_i\cdot\mathbf{r} = k\,x\cos\beta_i + k\,y\sin\beta_i$ does not depend on the z coordinate. This property implies that the light field exhibits translational invariance along the z direction, which corresponds to the lateral direction perpendicular to the inhomogeneous field plane. In addition, the vector $\boldsymbol{\mathcal{E}}_i = -m_i\sin\beta_i\mathbf{e}_x + m_i\cos\beta_i\mathbf{e}_y - \mathbf{e}_z$ characterizes the polarization of each wave with the complex polarization parameter m_i associated with the real normalized Stokes parameters defined as [1]

$$\tau_i = \frac{1-|m_i|^2}{1+|m_i|^2}, \quad \chi_i = \frac{2\,\mathrm{Re}\,m_i}{1+|m_i|^2}, \quad \sigma_i = \frac{2\,\mathrm{Im}\,m_i}{1+|m_i|^2}. \tag{2}$$

These parameters describe the different polarization states in the optical field. Specifically, the parameters $\tau_i = \pm 1$, $\chi_i = \pm 1$, and $\sigma_i = \pm 1$ represent the x (y) linear polarizations, 45° (−45°) linear polarizations, and right-hand (left-hand) circular polarizations, respectively.

The SAM density and complex Poynting momentum density are defined as [40,44,54,55]

$$\mathbf{s} = \frac{1}{4\omega}\,\mathrm{Im}\,(\varepsilon\mathbf{E}^*\times\mathbf{E} + \mu\mathbf{H}^*\times\mathbf{H}), \quad \widetilde{\mathbf{p}} = \frac{\varepsilon\mu}{2}\mathbf{E}^*\times\mathbf{H}, \tag{3}$$

where $\omega = k/\sqrt{\varepsilon\mu}$ is the angular frequency, and ε and μ denote the absolute permittivity and permeability of the background medium. The total SAM density $\mathbf{s}$ of the electromagnetic field, as described in Eq. (1), consists of two components: the L-spin density $\mathbf{s}_\mathrm{l}$ and T-spin density $\mathbf{s}_\mathrm{t}$ [1,2]. The T-spin density component emerges due to the nonuniform distribution of the total momentum density, represented by $\mathbf{s}_\mathrm{t} = \nabla\times\mathbf{p}/2k^2$, indicating T-spin-momentum locking [2,9]. The Poynting momentum density $\mathbf{p}$, consisting of the BSM density $\mathbf{p}_\mathrm{s}$ and orbital momentum density $\mathbf{p}_\mathrm{o}$, i.e., $\mathbf{p} = \mathrm{Re}\,\widetilde{\mathbf{p}} = \mathbf{p}_\mathrm{s} + \mathbf{p}_\mathrm{o}$ [44,55]. After a series of algebraic calculations, which are detailed in the Supplemental Material [56], the distribution of the L-spin density component can be derived as

$$\begin{aligned}\mathbf{s}_\mathrm{l} = \mathbf{s} - \mathbf{s}_\mathrm{t} = -\frac{\varepsilon}{8\omega}\sum_{i,j}^{n_p}\mathrm{Im}\left[U_i^* U_j (m_i^* - m_j) e^{-\mathrm{i}(\mathbf{k}_i-\mathbf{k}_j)\cdot\mathbf{r}}\right] \\ \times [1+\cos(\beta_i-\beta_j)] \\ \times [(\cos\beta_i+\cos\beta_j)\mathbf{e}_x + (\sin\beta_i+\sin\beta_j)\mathbf{e}_y].\end{aligned} \tag{4}$$

When setting $m_i^* - m_j = 0$, it leads to the elimination of the L-spin density in Eq. (4). However, the component of the total SAM density perpendicular to the wave propagation is independent of $m_i^* - m_j$ (see Eq. (S12) in the Supplemental Material [56]), retains as the pure T-spin density, i.e.,

$$\begin{aligned}\mathbf{s} = \mathbf{s}_\mathrm{t} &= -\frac{\varepsilon}{4\omega}\sum_{i,j}^{n_p}\sin(\beta_i-\beta_j)\,\mathrm{Im}\left[A_i^* A_j e^{\mathrm{i}(\mathbf{k}_i-\mathbf{k}_j)\cdot\mathbf{r}}\right]\mathbf{e}_z \\ &= -\frac{1}{\omega}\sum_{i,j}^{n_p}\tan\frac{\beta_i-\beta_j}{2}\,\mathrm{Im}(w_{ij})\mathbf{e}_z.\end{aligned} \tag{5}$$

The complex number w_{ij}, which is independent of m_i, is derived from the energy density of the interference field (see Eq. (S17) in the Supplemental Material [56]). Moreover, taking $m_i^* - m_j = 0$ into Eq. (2), the Stokes parameters become

$$\tau_i = \tau_j, \quad \chi_i = \chi_j, \quad \sigma_i = 0. \tag{6}$$

This implies that for each plane wave in the system, it is necessary for them to possess the same linear polarization state in order to attain a pure T spin. Then the total SAM density is perpendicular to the wave propagation and the inhomogeneous field plane and locked by the momentum density [2,10], as shown in Figs. 1 and 2.

Figures 2(a) and 2(b) illustrate the distribution of total SAM density and T-spin density, respectively (normalized to the maximum value of the SAM density). The spatial profiles in Figs. 2(a) and 2(b) are identical, implying a zero L-spin density and the optical field's total SAM density being solely contributed by the T-spin density. This is further verified by Fig. 2(c), which shows that the T-spin density (represented by dashed lines) coincides perfectly with the total SAM density (represented by double solid lines), thereby confirming

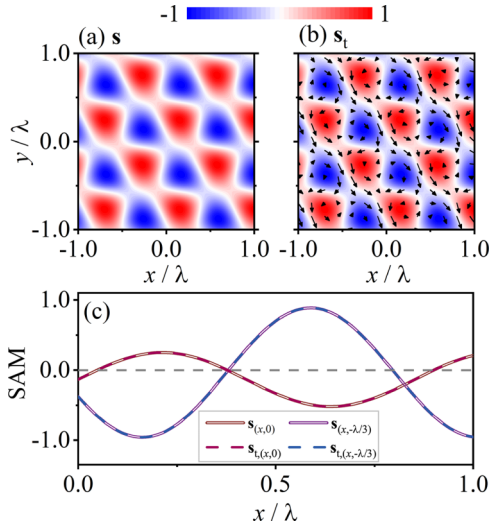

FIG. 2. The spatial profiles of the total SAM density $\mathbf{s}$, T-spin density $\mathbf{s}_t$ and the momentum density $\mathbf{p}$ in the interference field of three plane waves. The parameters of the plane waves in vacuum are set as $\lambda = 1000$ nm, $m_i = 1$, $A_i = 1$, i, $1 + \mathrm{i}$, and $\beta_i = 0°$, $100°$, $260°$ for $i = 1, 2, 3$, respectively. (a) The spatial profile of the normalized total SAM density. (b) Black arrows indicate the momentum-density vectors. The background intensity describes the distribution of normalized T-spin density derived from the momentum density's curl. (c) The normalized total SAM and T-spin density along the x direction when y is set to zero ($\mathbf{s}_{(x,0)}$ and $\mathbf{s}_{t,(x,0)}$) and $-\lambda/3$ ($\mathbf{s}_{(x,-\lambda/3)}$ and $\mathbf{s}_{t,(x,-\lambda/3)}$), respectively. The double solid lines expressing the total SAM density and the dashed lines representing the T-spin density show perfect agreement.

the presence of a pure T spin in the optical field. Furthermore, in contrast with the interference field with pure T spin, the spin density in the interference field generated by left circularly polarized plane waves ($m_i = \mathrm{i}$, $\sigma_i = 1$) is exhibited in Fig. 3. The landscapes of total SAM density, as visualized in Fig. 3(a), arises from the T spin and L spin. And the T spin and L spin have the similar relative magnitude in Figs. 3(b) and 3(c).

Next, let us focus on the characteristics of the complex Poynting momentum density $\tilde{\mathbf{p}}$. For an interference field consisting of multiple plane waves propagating in the same

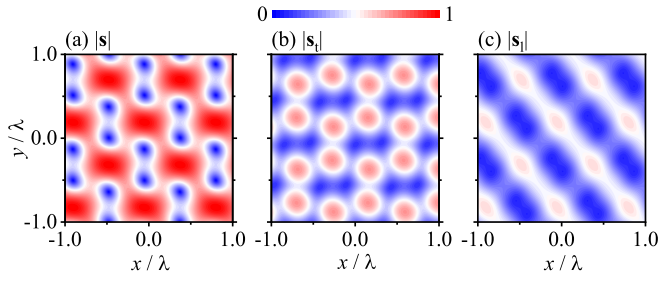

FIG. 3. Interference of three left circularly polarized plane waves with parameters the same as those used in Fig. 2, except for the complex number $m = \mathrm{i}$. The spatial profiles of the normalized spin density on the $z = 0$ plane, including the modulus of total SAM density $|\mathbf{s}|$ in panel (a), T-spin density $|\mathbf{s}_t|$ in panel (b), and L-spin density $|\mathbf{s}_l|$ in panel (c).

xy plane, the z component of the Poynting momentum density $\mathbf{p}$ is demonstrated to originate from the BSM density $\mathbf{p}_s$, expressed as

$$[\mathbf{p}]_z = [\mathbf{p}_s]_z = -\frac{\varepsilon}{4c}\sum_{i,j}^{n_p} \mathrm{Re}\left[U_i^* U_j (m_i^* - m_j) e^{-\mathrm{i}(\mathbf{k}_i - \mathbf{k}_j)\cdot\mathbf{r}}\right] \times \sin(\beta_i - \beta_j)\mathbf{e}_z. \quad (7)$$

Then in the scenario where $m_i^* - m_j = 0$, indicating that all plane waves have the same linear polarization and the optical field only possesses pure T spin, the z component of the momentum density becomes zero. This can be observed in Fig. 1, where the blue arrows represent the momentum density vectors of the interference field, and they are all confined to the xy plane. Similarly, in Fig. 2(b), the black arrows depict the momentum density vectors, which also lie within the xy plane. The alignment of these momentum density vectors in the field inhomogeneity plane (i.e., xy plane) confirms again that the T spin is restricted to the direction perpendicular to

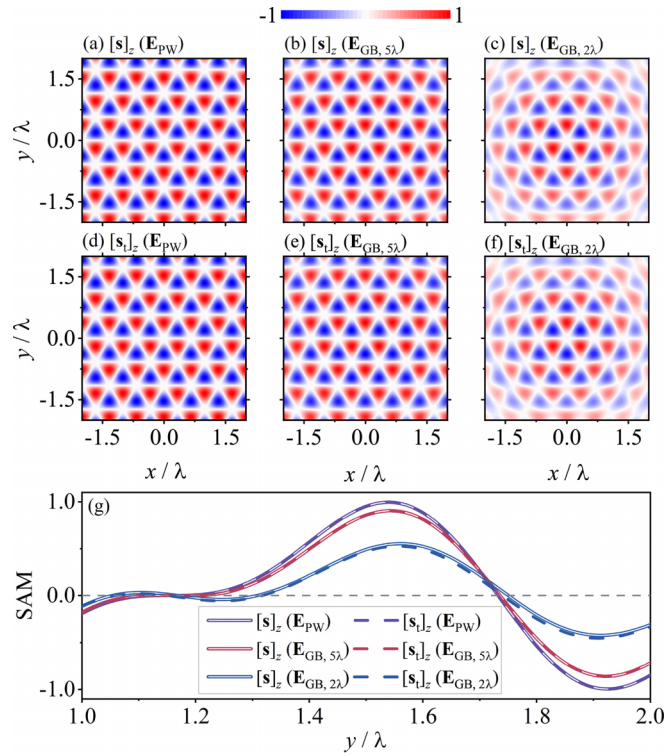

FIG. 4. (a) The spatial profiles of the normalized z component of the total SAM density in the optical lattice generated by the interference of three plane waves $\mathbf{E}_{PW}$ with the same polarization vector $m_i = 1$ and amplitude $A_i = \sqrt{2}$. The angles between the wave vectors of the plane waves and the x axis are $\beta_i = 0, 2\pi/3, 4\pi/3$ for $i = 1, 2, 3$, respectively. (b), (c) Replacement of the incident plane waves in panel (a) with Gaussian beams $\mathbf{E}_{GB}$ with the waist radius $\omega_0 = 5\lambda$ in panel (b), $\omega_0 = 2\lambda$ in panel (c). Distortion of the total SAM density distribution increases as the waist radius decreases. (d)–(f) The spatial profiles of the normalized z component of the T-spin density with parameters the same as those used in panels (a)–(c). (g) The z component of the total SAM and T-spin density on the y axis when x is set to zero. The double solid and dashed lines express the total SAM and T-spin densities, respectively.

the wave propagation and the inhomogeneous field plane, as indicated by the red arrows in Fig. 1. This alignment is a result of spin-momentum locking, a phenomenon where the direction of the spin (equals to T spin in this case) is coupled or "locked" to the direction of momentum.

On the other hand, in the case of interference field with pure T spin, we establish the relationship between the T-spin density and the imaginary Poynting momentum density (detailed in the Supplemental Material [56])

$$\mathrm{Im}\,\tilde{\mathbf{p}} = 2k\frac{m}{(1+m^2)}\mathbf{s}_\mathrm{t} - \frac{2k^2}{\omega}\sum_{i,j}^{n_p}\frac{\nabla\left(w_{ij}^{(\mathrm{e})} - w_{ij}^{(\mathrm{m})}\right)}{|\mathbf{k}_i - \mathbf{k}_j|^2}. \quad (8)$$

The imaginary Poynting momentum density has been demonstrated to be responsible for various intriguing optical force and torque phenomena [45,46]. Equation (8) opens up opportunities to study and understand the intricate interplay between T spin and optical forces, allowing for the investigation of a wide range of attractive optical phenomena associated with T spin. In the evanescent wave with pure T spin, the curl part of the imaginary Poynting momentum density also corresponds to the T spin density, which was discussed in our previous work [47].

As an additional example, in an optical lattice field comprising three plane waves $\mathbf{E}_\mathrm{PW}$, we present the spatial profiles of total SAM density in Fig. 4(a) and T-spin density in Fig. 4(d) (normalized to the maximum value of the SAM density), each plane wave with the same polarization vector $m_i = 1$ and an amplitude $A_i = \sqrt{2}$. The wave vectors' angles with respect to the x axis are $\beta_i = 0,\ 2\pi/3,\ 4\pi/3$ for $i = 1, 2, 3$, respectively. Furthermore, we have investigated the z component of the total SAM and T-spin density in a quasi-optical lattice generated by Gaussian beams $\mathbf{E}_\mathrm{GB}$ with optical axes situated in the $z = 0$ plane. In contrast with the scenario involving plane waves, when comparing Fig. 4(e) with Fig. 4(f), we observe that the distortion in the pure T-spin density resulting from the interference of Gaussian beams becomes more prominent as the beam waist radius (ω_0) decreases. Figure 4(g) illustrates the variation of the z component of the total SAM (represented by double solid lines) and T-spin density (represented by dashed lines) along the y axis at $x = 0$ in the quasi-optical lattice. The distribution of SAM density deviates as the position moves away from the center of the optical field. When considering an infinite beam waist radius, these expressions go back to the case in the optical lattice. Remarkably, even with a narrow waist radius ($\omega_0 = 2\lambda$), the T-spin density closely aligns with the total SAM density, underscoring the robustness of pure T spin in the interference field. This robustness further suggests that a range of fields with pure T spin hold significant potential for experimental detection.

Conclusion. To summarize, we have successfully demonstrated both analytically and numerically the presence of a pure T spin in optical fields with translational invariance. This phenomenon occurs when an interference field is formed by multiple plane waves with the same linear polarization state. The optical field interference disrupts the uniform distribution of momentum in the xy plane. Consequently, a T-spin density arises and is directed along the direction perpendicular to the wave propagation and the inhomogeneous field plane. The physical properties of the individual plane waves in generating pure T spin, apart from having the same frequency and polarization state, can be arbitrary. This characteristic ensures the high universality of our analysis. By selecting a certain polarization, we achieve a pure T spin while simultaneously eliminating the lateral BSM. This provides a unique mechanical property in the lateral direction, deepening our understanding of spins and offering new avenues for spin-based applications.

Acknowledgments. This work was supported by the National Natural Science Foundation of China (Grants No. 12074084, No. 12174231, and No. 62375245), National Key R&D Program of China (Grants No. 2018YFA0306201 and No. 2016YFA0301103). Shanxi Province 100-Plan Talent Program, Fundamental Research Program of Shanxi Province through 202103021222001.

[1] K. Y. Bliokh and F. Nori, Transverse and longitudinal angular momenta of light, Phys. Rep. **592**, 1 (2015).
[2] P. Shi, L. Du, C. Li, A. V. Zayats, and X. Yuan, Transverse spin dynamics in structured electromagnetic guided waves, Proc. Natl. Acad. Sci. USA **118**, e2018816118 (2021).
[3] A. Fert, Nobel lecture: Origin, development, and future of spintronics, Rev. Mod. Phys. **80**, 1517 (2008).
[4] L. Allen, S. M. Barnett, and M. J. Padgett, *Optical Angular Momentum* (CRC Press, Boca Raton, 2016).
[5] K. Y. Bliokh, F. J. Rodríguez-Fortuño, F. Nori, and A. V. Zayats, Spin-orbit interactions of light, Nat. Photon. **9**, 796 (2015).
[6] K. Y. Bliokh, H. Punzmann, H. Xia, F. Nori, and M. Shats, Field theory spin and momentum in water waves, Sci. Adv. **8**, eabm1295 (2022).
[7] S. Golat, E. A. Lim, and F. J. Rodríguez-Fortuño, Evanescent gravitational waves, Phys. Rev. D **101**, 084046 (2020).
[8] S. Xin, Y. Long, and J. Ren, Spin angular momentum of gravitational wave interference, New J. Phys. **23**, 043035 (2021).
[9] P. Shi, L. Du, and X. Yuan, Spin photonics: From transverse spin to photonic skyrmions, Nanophotonics **10**, 3927 (2021).
[10] P. Shi, L. Du, A. Yang, X. Yin, X. Lei, and X. Yuan, Dynamical and topological properties of the spin angular momenta in general electromagnetic fields, Commun. Phys. **6**, 283 (2023).
[11] V. B. Berestetskii, E. M. Lifshitz, and L. P. Pitaevskii, *Quantum Electrodynamics* (Pergamon Press, Oxford, 1982), Vol. 4.
[12] F. D. M. Haldane and S. Raghu, Possible realization of directional optical waveguides in photonic crystals with broken time-reversal symmetry, Phys. Rev. Lett. **100**, 013904 (2008).
[13] T. Ozawa, H. M. Price, A. Amo, N. Goldman, M. Hafezi, L. Lu, M. C. Rechtsman, D. Schuster, J. Simon, O. Zilberberg, and I. Carusotto, Topological photonics, Rev. Mod. Phys. **91**, 015006 (2019).

[14] Z. Wang, Y. Chong, J. D. Joannopoulos, and M. Soljačić, Observation of unidirectional backscattering-immune topological electromagnetic states, Nature (London) **461**, 772 (2009).

[15] M. Antognozzi, C. Bermingham, R. Harniman, S. Simpson, J. Senior, R. Hayward, H. Hoerber, M. Dennis, A. Bekshaev, K. Bliokh, and F. Nori, Direct measurements of the extraordinary optical momentum and transverse spin-dependent force using a nano-cantilever, Nat. Phys. **12**, 731 (2016).

[16] S. Chu, Nobel lecture: The manipulation of neutral particles, Rev. Mod. Phys. **70**, 685 (1998).

[17] R. W. Bowman and M. J. Padgett, Optical trapping and binding, Rep. Prog. Phys. **76**, 026401 (2013).

[18] M. Dienerowitz, M. Mazilu, and K. Dholakia, Optical manipulation of nanoparticles: A review, J. Nanophotonics **2**, 021875 (2008).

[19] D. G. Grier, A revolution in optical manipulation, Nature (London) **424**, 810 (2003).

[20] Y. Shi, X. Xu, M. Nieto-Vesperinas, Q. Song, A. Q. Liu, G. Cipparrone, Z. Su, B. Yao, Z. Wang, C.-W. Qiu, and X. Cheng, Advances in light transverse momenta and optical lateral forces, Adv. Opt. Photonics **15**, 835 (2023).

[21] A. Ashkin, History of optical trapping and manipulation of small-neutral particle, atoms, and molecules, IEEE J. Sel. Top. Quantum Electron. **6**, 841 (2000).

[22] T. Van Mechelen and Z. Jacob, Universal spin-momentum locking of evanescent waves, Optica **3**, 118 (2016).

[23] G. Araneda, S. Walser, Y. Colombe, D. B. Higginbottom, J. Volz, R. Blatt, and A. Rauschenbeutel, Wavelength-scale errors in optical localization due to spin-orbit coupling of light, Nat. Phys. **15**, 17 (2019).

[24] J. Zhou, H. Qian, C. F. Chen, J. Zhao, G. Li, Q. Wu, H. Luo, S. Wen, and Z. Liu, Optical edge detection based on high-efficiency dielectric metasurface, Proc. Natl. Acad. Sci. USA **116**, 11137 (2019).

[25] J. Zhou, S. Liu, H. Qian, Y. Li, H. Luo, S. Wen, Z. Zhou, G. Guo, B. Shi, and Z. Liu, Metasurface enabled quantum edge detection, Sci. Adv. **6**, eabc4385 (2020).

[26] Z. Shao, J. Zhu, Y. Chen, Y. Zhang, and S. Yu, Spin-orbit interaction of light induced by transverse spin angular momentum engineering, Nat. Commun. **9**, 926 (2018).

[27] O. Y. Yermakov, A. I. Ovcharenko, A. A. Bogdanov, I. V. Iorsh, K. Y. Bliokh, and Y. S. Kivshar, Spin control of light with hyperbolic metasurfaces, Phys. Rev. B **94**, 075446 (2016).

[28] Y. Mazor and A. Alù, Routing optical spin and pseudospin with metasurfaces, Phys. Rev. Appl. **14**, 014029 (2020).

[29] C. C. Li, P. Shi, L. P. Du, and X. C. Yuan, Mapping the near-field spin angular momenta in the structured surface plasmon polariton field, Nanoscale **12**, 13674 (2020).

[30] X. Piao, S. Yu, and N. Park, Design of transverse spinning of light with globally unique handedness, Phys. Rev. Lett. **120**, 203901 (2018).

[31] P. Shi, H. Li, L. Du, and X. Yuan, Spin-momentum properties in the paraxial optical systems, ACS Photonics **10**, 2332 (2023).

[32] Y. Pan, X.-Z. Gao, G.-L. Zhang, Y. Li, C. Tu, and H.-T. Wang, Spin angular momentum density and transverse energy flow of tightly focused kaleidoscope-structured vector optical fields, APL Photonics **4**, 096102 (2019).

[33] J. Chen, C. Wan, L. J. Kong, and Q. Zhan, Tightly focused optical field with controllable photonic spin orientation, Opt. Express **25**, 19517 (2017).

[34] V. V. Kotlyar, A. G. Nalimov, A. A. Kovalev, A. P. Porfirev, and S. S. Stafeev, Spin-orbit and orbit-spin conversion in the sharp focus of laser light: Theory and experiment, Phys. Rev. A **102**, 033502 (2020).

[35] A. Aiello, P. Banzer, M. Neugebauer, and G. Leuchs, From transverse angular momentum to photonic wheels, Nat. Photon. **9**, 789 (2015).

[36] L. Hang, J. Fu, X. Yu, Y. Wang, and P. Chen, Generation of a sub-half-wavelength focal spot with purely transverse spin angular momentum, Appl. Phys. B: Lasers Opt. **123**, 266 (2017).

[37] M. Neugebauer, S. Grosche, S. Rothau, G. Leuchs, and P. Banzer, Lateral spin transport in paraxial beams of light, Opt. Lett. **41**, 3499 (2016).

[38] A. Y. Bekshaev, K. Y. Bliokh, and F. Nori, Transverse spin and momentum in two-wave interference, Phy. Rev. X **5**, 011039 (2015).

[39] K. Y. Bliokh, A. Y. Bekshaev, and F. Nori, Optical momentum, spin, and angular momentum in dispersive media, Phys. Rev. Lett. **119**, 073901 (2017).

[40] K. Y. Bliokh, A. Y. Bekshaev, and F. Nori, Extraordinary momentum and spin in evanescent waves, Nat. Commun. **5**, 3300 (2014).

[41] K. Y. Bliokh, D. Smirnova, and F. Nori, Quantum spin Hall effect of light, Science **348**, 1448 (2015).

[42] F. J. Belinfante, On the current and the density of the electric charge, the energy, the linear momentum and the angular momentum of arbitrary fields, Physica **7**, 449 (1940).

[43] K. Mita, Virtual probability current associated with the spin, Am. J. Phys. **68**, 259 (2000).

[44] M. V. Berry, Optical currents, J. Opt. A **11**, 094001 (2009).

[45] X. Xu and M. Nieto-Vesperinas, Azimuthal imaginary Poynting momentum density, Phys. Rev. Lett. **123**, 233902 (2019).

[46] Y. Zhou, X. Xu, Y. Zhang, M. Li, S. Yan, M. Nieto-Vesperinas, B. Li, C.-W. Qiu, and B. Yao, Observation of high-order imaginary Poynting momentum optomechanics in structured light, Proc. Natl. Acad. Sci. USA **119**, e2209721119 (2022).

[47] X. Yu, Y. Li, B. Xu, X. Wang, L. Zhang, J. Chen, Z. Lin, and C. T. Chan, Anomalous lateral optical force as a manifestation of the optical transverse spin, Laser Photonics Rev. **17**, 2300212 (2023).

[48] A. Derevianko and H. Katori, Colloquium: Physics of optical lattice clocks, Rev. Mod. Phys. **83**, 331 (2011).

[49] P. Jessen and I. Deutsch, Optical lattices, Adv. At. Mol. Opt. Phys. **37**, 95 (1996).

[50] Y. Jiang, H. Lin, X. Li, J. Chen, J. Du, and J. Ng, Hidden symmetry and invariance in optical forces, ACS Photonics **6**, 2749 (2019).

[51] L. Allen, M. W. Beijersbergen, R. J. C. Spreeuw, and J. P. Woerdman, Orbital angular momentum of light and the transformation of Laguerre-Gaussian laser modes, Phys. Rev. A **45**, 8185 (1992).

[52] M. Neugebauer, T. Bauer, A. Aiello, and P. Banzer, Measuring the transverse spin density of light, Phys. Rev. Lett. **114**, 063901 (2015).

[53] M. Born and E. Wolf, *Principles of Optics* (Cambridge University Press, Cambridge, 2013).

[54] J. D. Jackson, *Classical Electrodynamics* (Wiley, New York, 1999).

[55] A. Y. Bekshaev and M. S. Soskin, Transverse energy flows in vectorial fields of paraxial beams with singularities, Opt. Commun. **271**, 332 (2007).

[56] See Supplemental Material at http://link.aps.org/supplemental/10.1103/PhysRevB.108.L241112 for (I) electromagnetic field quantities of the interference field, (II) transverse spin in multiple plane waves, (III) complex Poynting momentum in multiple plane waves, (IV) pure transverse spin in the optical lattice and Gaussian beams, which includes Refs. [1,2,9,26,38,40,44,45,49,53–55,57–67].

[57] H. Kogelnik and T. Li, Laser beams and resonators, Appl. Opt. **5**, 1550 (1966).

[58] P. C. Chaumet, Fully vectorial highly nonparaxial beam close to the waist, J. Opt. Soc. Am. A **23**, 3197 (2006).

[59] A. Y. Bekshaev, Subwavelength particles in an inhomogeneous light field: Optical forces associated with the spin and orbital energy flows, J. Opt. (Bristol, UK) **15**, 044004 (2013).

[60] D. E. Soper, *Classical Field Theory* (Dover Publications, New York, 2008).

[61] R. Baierlein, Representing a vector field: Helmholtz's theorem derived from a Fourier identity, Am. J. Phys. **63**, 180 (1995).

[62] P. Vaveliuk, B. Ruiz, and A. Lencina, Limits of the paraxial approximation in laser beams, Opt. Lett. **32**, 927 (2007).

[63] S. Albaladejo, M. I. Marqués, M. Laroche, and J. J. Sáenz, Scattering forces from the curl of the spin angular momentum of a light field, Phys. Rev. Lett. **102**, 113602 (2009).

[64] X. Yu, Y. Jiang, H. Chen, S. Liu, and Z. Lin, Approach to fully decomposing an optical force into conservative and nonconservative components, Phys. Rev. A **100**, 033821 (2019).

[65] M. Greiner and S. Fölling, Optical lattices, Nature (London) **453**, 736 (2008).

[66] Y. Jiang, H. Chen, J. Chen, J. Ng, and Z. Lin, Universal relationships between optical force/torque and orbital versus spin momentum/angular momentum of light, arXiv:1511.08546.

[67] T. A. Al-Saeed, Modeling Gaussian beam focusing by the Poynting vector in Monte Carlo simulation and a concise review, Optik (Munich, Ger.) **177**, 71 (2019).